Numerical Simulation of Wave Scattering at Shock-Loaded Metallic Plates and Shells in Water

Peter Voinovich[1,2], Alan Merlen[2], Eugene Timofeev[1], and Kazuyoshi Takayama[1]

[1] Shock Wave Research Center, IFS, Tohoku University, Sendai 980-8577, Japan
[2] Laboratoire de Mécanique de Lille, 59655 Villeneuve d'Ascq Cedex, France

Abstract. A 2D numerical model to simulate elastic waves in solids and liquids has been developed and thoroughly tested. The equations of motion are written in terms of stresses, displacements and displacement velocities for control volumes constructed about the nodes of a triangular unstructured grid. Theoretical dispersion for zero mode symmetric (S_0) and antisymmetric (A_0) Lamb waves in a plate has been reproduced numerically with high accuracy. Comparison of simulated acoustic pulse scattering at water-immersed steel plate with the respective experiment reveals a very good agreement in such delicate features as excitation of the surface wave (A). An example of acoustic pulse interaction with a curvilinear metallic shell in water demonstrates flexibility of the method with respect to complex geometries.

1 Introduction

The aim of the present work is to develop a numerical tool based directly on the equation of motion and capable of simulating propagation of acoustic pulses through essentially inhomogeneous elastic media including solids and liquids. At this stage, we confine ourselves to two spatial dimensions. The equation of motion written in displacements/stresses terms is selected to obtain a highly universal method easily allowing further upgrades to incorporate various kinds of non-linearities in the displacement-stress relations. The unstructured grid system based on triangular area elements has been adopted for domain discretization to allow highest flexibility in description of various geometries of interest including internal boundaries separating sub-domains with different elastic properties.

2 Numerical Method

The equations of motion of a volume V bounded by surface S, with no volume forces applied, can be written in the most general integral form as follows ([1]):

$$\int_V \rho \ddot{U}_l \, \mathrm{d}v = \oint_S \sigma_{lm} \, n_m \, \mathrm{d}s \quad , \tag{1}$$

U_l being Cartesian projections of the displacement vector $\mathbf{U}$, ρ – density, σ_{lm} – components of the stress tensor, and n_m – Cartesian projections of the outward

normal $\mathbf{n}$ to the surface S (i.e. in two dimensions $l = x, y$ and $m = x, y$; summation over m is assumed). In an isotropic elastic medium under small strain, the components of the stress tensor depend linearly on deformation:

$$\sigma_{xx} = 2\mu\frac{\partial U_x}{\partial x} + \lambda\left(\frac{\partial U_x}{\partial x} + \frac{\partial U_y}{\partial y}\right) \ , \quad \sigma_{xy} = \mu\left(\frac{\partial U_x}{\partial y} + \frac{\partial U_y}{\partial x}\right) \ , \qquad (2)$$

$$\sigma_{yy} = 2\mu\frac{\partial U_y}{\partial y} + \lambda\left(\frac{\partial U_x}{\partial x} + \frac{\partial U_y}{\partial y}\right) \ , \quad \mu = \frac{1}{2}K\frac{(1 - 2\nu)}{(1 + \nu)} \ , \quad \lambda = K\frac{\nu}{(1 + \nu)} \ .$$

Here μ and λ are the Lamé constants which depend on the elastic properties: K being the modulus of compression, and ν – Poisson's ratio ($0 < \nu \leq 1/2$). The above formulas are universally valid for both elastic solids and liquids (assuming negligible convection). The latter are presented by $\nu = 1/2$, $K = \rho_0 c_0^2$, where ρ_0 is liquid's density and c_0 – the sound speed, so that $\mu = 0$ and $\lambda = \rho_0 c_0^2/3$.

The unstructured grid generator [2] has been used in this work to generate the grid composed of triangular area elements for a given computational domain in 2-D. It automatically inserts nodes and triangulates a set of adjoined sub-domains ensuring exact matching of nodes in the resulting sub-grids at the internal boundaries to facilitate setting up proper internal boundary conditions. The grid generation can be performed either for a set of uniformly distributed
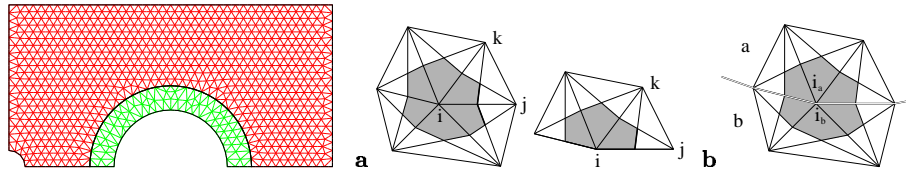

Fig. 1. Simple grid for two sub-domains with matching nodes at internal boundaries

Fig. 2. (a) Control volumes about internal and boundary nodes; the interface between neighbor nodes i and j is shown in bold line. (b) "Twin" nodes at an internal boundary between sub-domains a and b.

nodes or by incremental insertion of new nodes until the maximum grid spacing meets the prescribed value. A version of the algorithm [3] has been employed with subsequent iterative improvement of grid quality by stretching and swapping of edges. An example of a simple grid for two sub-domains with curvilinear internal boundaries is presented in Fig. 1 (actual grids typically contain many more nodes). The node-centered technique for establishing control volumes has been selected. The dual grid of control volumes is created by connecting triangles' centroids with the centers of their edges (Fig. 2a).

The numerical scheme is based on equations (1) written for the control volumes (Fig. 2a). The Cartesian projections of displacements (U_x, U_y) and displacement velocities ($\dot{U}_x$, $\dot{U}_y$) are given for the time moment t^n at grid nodes. To advance the solution one time step Δt, first, derivatives $\partial U_x/\partial x$, $\partial U_y/\partial x$,

$\partial U_x / \partial y$, $\partial U_y / \partial y$, are computed by Lagrange interpolation for every grid triangle using predicted values for displacements at time $t^{n+1/2} = t^n + \Delta t / 2$:

$$\left(\frac{\partial U_\alpha}{\partial x} \right)^{n+1/2} \approx \left[(y_k - y_i)(U_{\alpha\,j}^{n+1/2} - U_{\alpha\,i}^{n+1/2}) - (y_j - y_i)(U_{\alpha\,k}^{n+1/2} - U_{\alpha\,i}^{n+1/2}) \right] / D \ ,$$

$$\left(\frac{\partial U_\alpha}{\partial y} \right)^{n+1/2} \approx \left[(x_k - x_i)(U_{\alpha\,j}^{n+1/2} - U_{\alpha\,i}^{n+1/2}) - (x_j - x_i)(U_{\alpha\,k}^{n+1/2} - U_{\alpha\,i}^{n+1/2}) \right] / D \ ,$$

where $D = (x_j - x_i)(y_k - y_i) - (y_j - y_i)(x_k - x_i)$, $U_{\alpha\,i}^{n+1/2} = U_{\alpha\,i}^n + 0.5\,\Delta t\,\dot{U}_{\alpha\,i}^n$, and $\alpha = x, y$. Components of the stress tensor $\sigma_{xx}^{n+1/2}$, $\sigma_{xy}^{n+1/2}$, $\sigma_{yy}^{n+1/2}$ are computed then according to equations (2) for every grid triangle.

Assuming uniform stress values within a grid triangle, equations (1) can be used in the following discrete form to calculate accelerations of grid nodes:

$$\left(\dot{U}_{\alpha\,i}^{n+1} - \dot{U}_{\alpha\,i}^n \right) V_i \, \rho_i = \Delta t \sum_{S_i} \sigma_{\alpha x} \Delta S_x + \sigma_{\alpha y} \Delta S_y \ , \tag{3}$$

where summation is performed over all the surface segments of control volume i. Finally, new displacements at time t^{n+1} can be computed for the grid nodes:

$$U_{\alpha\,i}^{n+1} = U_{\alpha\,i}^n + \Delta t\,\dot{U}_{\alpha\,i}^{n+1} \ . \tag{4}$$

In all practical computations, the described explicit scheme was found conditionally stable in accordance with the CFL criterion.

The following two types of boundary conditions can be directly applied within the described simulation algorithm at the external boundaries of a computational domain: the displacement velocities or surface forces can be given as functions of time at boundary nodes or boundary surface segments, respectively. The boundary displacement velocities are substituted into equations (4), while the surface forces are used at the surface segments of control volumes in (3). A stress-free surface, for example, is simulated by applying zero surface forces at its boundary segments, while zero normal displacements and displacement velocities correspond to the slip condition at an absolutely rigid wall or symmetry plane. The internal boundaries between sub-domains in contact represent a special case. A wide variety of boundary conditions can be set up there, including the non-slip or slip ones with or without friction, a gap opening etc. To support various boundary conditions at the internal boundaries in the described numerical model, matching ("twin") nodes are used at the common sub-domains' borders (Fig. 1): a node i_a at the internal boundary of sub-domain a in contact with sub-domain b has a respective matching node i_b of sub-domain b (Fig. 2b).

In the following examples of solid plates and shells in liquid, the "twin" nodes were processed to simulate the inviscid slip boundary condition. It has been achieved by setting up zero friction forces at the boundary and by equalizing displacements and displacement velocities in the normal direction. The resulting averaged normal displacements and displacement velocities $N_{i(a),i(b)}$ at "twin" nodes i_a and i_b accumulate preliminary computed individual values $N_{i(a)}$ and $N_{i(b)}$ as follows: $N_{i(a),i(b)} \left(\int\limits_{V_i(a)} \rho_a \; \mathrm{d}v + \int\limits_{V_i(b)} \rho_b \; \mathrm{d}v \right) = N_{i(a)} \int\limits_{V_i(a)} \rho_a \; \mathrm{d}v + N_{i(b)} \int\limits_{V_i(b)} \rho_b \; \mathrm{d}v \ .$

3 Lamb Waves in a Plate

Elastic waves in a plate in vacuum under periodic harmonic excitation have been selected as a primary test case for the developed method and code. Examples of waves in a plate under uniform harmonic longitudinal and transversal excitation at the left hand side are presented in Fig. 3a,b in the form of compression diagrams, i.e. negative values of $\sigma_{xx} + \sigma_{yy}$ are given in dark gray and black (compression), while positive values – in light gray and white (decompression). Each figure presents the same two successive moments in time after the excitation started. Normal displacements of the upper and lower surfaces are shown exaggerated enormously for demonstration. Different modes of waves can be seen in either case propagating at different speeds along the plate. Results presented in Fig. 3a and b correspond to identical dimensionless excitation frequency $(\omega h)/(\pi C_L) = 0.4$, $2h$ being the plate thickness and C_L – velocity of the longitudinal wave. The dominant waves seen in the figures are the lowest symmetric (S_0 in Fig. 3a) and the lowest antisymmetric (A_0 in Fig. 3b) Lamb waves. One can note higher phase velocity of S_0 compared to A_0, as longer waves are generated in the former case. On the contrary, the group velocity is higher for A_0, so that the periodic wave pattern advances faster in this case resulting in considerably larger number of periods observed at a certain moment after the onset of excitation. In both cases, the compression/decompression pattern at the latter time moment is spoiled by the effect of reflection at the right-hand side of the plate. The observed relations between the wave's velocities are consistent with the theory [1].

Simulations have been performed for a wide range of excitation parameters using a rather coarse grid containing only 10 internal nodes across the plate. Propagation velocities for S_0, A_0, longitudinal, transversal and Rayleigh waves extracted from the numerical solutions for a steel plate ($\rho = 7.9 \cdot 10^3$ kg/m^3, $\sigma = 0.29$, $C_L = 5790$ m/s) along with the theoretical dispersion curves for S_0, A_0 are presented in Fig. 4. The longitudinal waves were simulated by uniform longitudinal (x-direction) excitation and zero normal displacements set up at the upper and lower boundaries. Transversal (y-direction) excitation and zero tangential displacements at the plate upper and lower boundaries were used for the transversal (shear) wave. The stress-free boundary conditions together with longitudinal or transversal excitation were used to observe symmetric (S_n) or antisymmetric (A_n) waves respectively. The quasi-Rayleigh waves appeared in the solution at high excitation frequencies as stable wave patterns in surface displacements whose shape did not vary essentially with propagation. Different symbols in the plot correspond to different modes of data processing. Position of the leading signal at a fixed time can be used to determine phase/group velocity of non-dispersive waves (squares). Two major methods applicable to all types of waves are based on measuring the wave length at a given time moment (triangles) or the slope of wave patterns on the displacement carpet diagrams (circles).
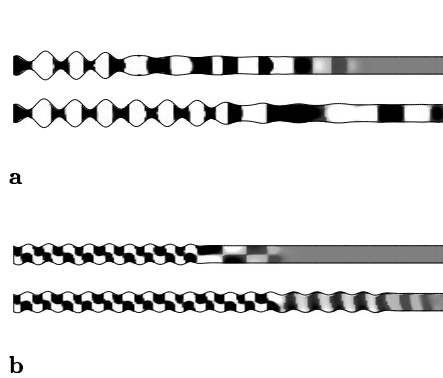
Fig. 3. Compression diagrams for computed symmetric (**a**) and antisymmetric (**b**) waves in elastic plate by uniform harmonic longitudinal (**a**) and transversal (**b**) excitation at the left-hand side. Surface displacements shown amplified for visualization.
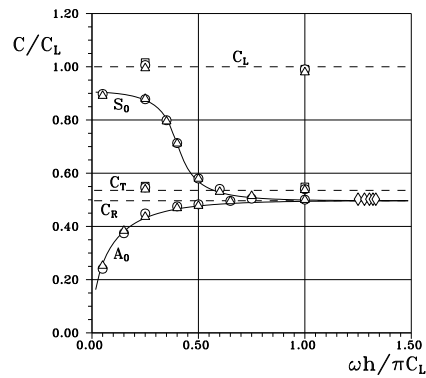
Fig. 4. Computed phase velocities (symbols) for S_0 and A_0 Lamb waves, quasi-Rayleigh (C_R; diamonds) waves, longitudinal (C_L) and transversal (C_T) waves in a steel plate versus theory ([1,4]; solid lines). Dashed lines indicate exact values of C_L, C_T, and C_R.

4   Steel Plate in Water

If a plate or shell is submerged in liquid, then waves propagating in the solid radiate into the surrounding medium. In addition to the regular compression waves propagating through the liquid at the sound speed C_0, an inhomogeneous surface wave A (the Scholte-Stoneley wave) can be observed in some cases propagating in the liquid close to the solid surface at a speed somewhat less than C_0. An example of experimental observation of this wave is given in Fig. 5 as a shadowgraph of waves in water close to the surface of a steel shell after excitation by an acoustic pulse. First, the surface wave in water appears as a distortion in waves radiated by A_0 in the shell (Fig. 5, top). Later on, the surface wave becomes more distinctive (Fig. 5, bottom).

Our numerical simulation was performed for a steel plate in contact with water. The grid contained two sub-domains representing the plate and the water volume. A sharp variation in normal displacements was applied at a small area of the water-solid boundary close to the plate's end to excite waves in the plate. Fig. 6 presents some results as compression diagrams (dark regions corresponding to higher pressure) for a few successive time moments. Formation of the surface wave in water (Sholte-Stoneley, A wave) can be seen in its development. S_0 and A_0 waves propagate along the plate and radiate into water. The radiation pattern for A_0 wave looks very similar to that in the experiment (Fig. 5; radiation by S_0 is out of the view field). The leading signal related to A_0 propagates at a constant speed which corresponds to the group velocity and is essentially higher than the sound speed in water. As a result, the front

of disturbances in water produced by A_0 is straight. A 90° phase shift can be observed between the compression extrema in plate and in water, as maximum compression at the upper plate's surface corresponds to the maximal negative displacement (see Fig. 3b), while due to the supersonic propagation velocity relative to C_0, maximum compression in water is generated by maximum variation in the displacement. The propagation velocity of A_0 decreases continuously due to dispersion, so that radiated waves become curved. The phase shift for slower waves diminishes. At a certain moment, the propagation speed of the rear part of A_0 with largest wave length equalizes with the sound speed in water. The phase shift between the compression extrema in water and plate vanishes. While decreasing further, the speed of A_0 becomes equal to that of the surface wave A in water, at which point a part of early radiated waves start propagating in a new mode involving the underlying elastic solid. A sharp phase shift arises consequently in the compression field in water.
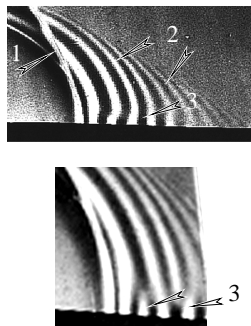

Fig. 5. Scholte-Stoneley wave in water near a steel shell hit by an acoustic pulse. 1 – the incident wave, 2 – waves radiated by A_0 in the shell, 3 – the Scholte-Stoneley (A) wave in water.
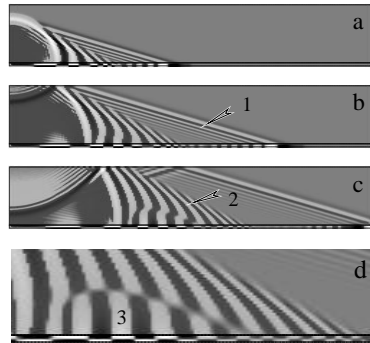

Fig. 6. Simulated radiation into water by S_0 (1) and A_0 (2) in a steel plate and emerging of surface wave A (3). Sequential compression diagrams for the whole computational domain (**a** – **c**) and a detail (**d**).

5   Cylindric Shell in Water

Experiments and some theory on the scattering of a short acoustic pulse at cylindrical shells in water have been reported by [5]. A typical shadowgraph from these experiments for an empty steel shell with the inner-to-outer radius ratio of 0.94 is presented in Fig. 7a. The two kind of waves in the shell traveling ahead of the incident pulse and radiating into water have been identified as zero mode symmetric (S_0) and antisymmetric (A_0) Lamb waves. A computational grid similar to that shown in Fig. 1 but with much finer spacing ($\approx 78,000$ total nodes) has been used in computations. A snapshot of the numerical result in a
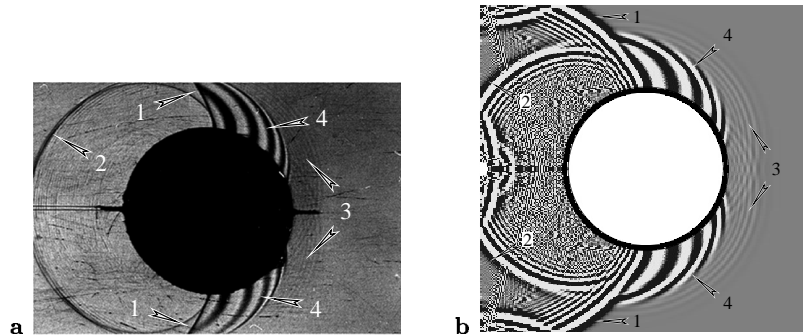
Fig. 7. Experimental [5] and computational shadowgraph of waves in water around an empty cylindrical shell by impulsive acoustic loading; 1 – incident pulse wave, 2 – reflected wave, 3 – radiation by S_0 in the shell, 4 – radiation by A_0 in the shell.

form of computer-generated shadowgraph is given in Fig. 7b. The waves radiated into water by the Lamb waves in the shell appear well captured (compare Fig. 7a and Fig. 7b). Oscillations of numerical nature are seen behind the incident and reflected wave fronts in water. The high-frequency numerical noise behind the reflected wave has a very small amplitude and becomes visible due to the post-processing technique sensitive to the second derivatives of the solution.

6   Conclusion

A numerical technique based on the direct application of the equations of motion, written in a general integral form in terms of stresses, displacements and displacement velocities, to control volumes constructed about the nodes of a triangular unstructured grid, has been developed and thoroughly tested against theory and experimental data. A good agreement with the experiment has been achieved for a pulse wave scattering at the water-immersed steel shell. Excitation of the Scholte-Stoneley surface wave via the waves radiated into water by the dispersive lowest antisymmetric Lamb wave (A_0) in a steel plate has been observed and analyzed in detail, explaining the experimental data.

References

1. L. Brekhovskih and V. Goncharov: *Mechanics of Continua and Wave Dynamics* (Springer-Verlag 1985)
2. A. Galyukov and P. Voinovich: '2-D triangular unstructured grid generator for multiple sub-domains', Soft-Impact Ltd., St. Petersburg, Russia (1997, unpublished)
3. D.F. Watson: The Computer Journal, **24**(2), 167 (1981)
4. L.M. Brekhovskikh: *Waves in Layered Media* (Academic Press 1960)
5. A.C. Ahyi, P. Pernod, O. Gatti et al.: J. Acoust. Soc. Am., **104**(5), 2727 (1998)